Exp. Theo. NANOTECHNOLOGY 10 (2026) 693-707 https://doi.org/10.56053/10.2.693

Characterization of single and multiple SnO_2 and MWCNTs nanocompsite with polythiophene (PTh) for NO_2 gas sensor

Faten A. Jasim[1,], Thamir A. A. Hassan[1], Muntadher I. Rahmah[2]*

[1]Department of Physics, College of Science, University of Baghdad, Baghdad, Iraq
[2]Department of Physics, College of Science, University of Al-Karkh, Baghdad, Iraq
[*]) Email: Faten.Adnan1104a@sc.uobaghdad.edu.iq

Received 6/2/2026, *Received in revised form* 25/3/2026, *Accepted* 29/3/2026, *Published* 15/4/2026

In this study, nanocomposites are made by chemical polymerization technique, adding different percentages of MWCNT nanoparticles and SnO_2 nanoparticles and studying their effect on the nanocomposite, where the results of the XRD tests are shown. It indicates the presence of clear diffraction peaks due to MWCNT and SnO_2. The surface morphology of the pure polymer has changed after adding fixed concentrations of SnO_2 and MWCNT, according to the FE-SEM data. The FTIR analysis revealed the kinds and concentrations of the components included in the nanocomposite and the sample's suitability for various applications. After that, the Nan composites will be deposed on the glass substrate for testing as NO_2 gas sensors with different temperatures. Let us get the best sensitivity at 150 ºC.

Keywords: Polythiophene; Polythiophene; $MWCNT_S$; SnO_2; Gas sensor.

1. INTRODUCTION

Currently, there is significant emphasis on the development of organic-inorganic nanocomposites. Two methods exist to achieve this: grafting synthetic polymers onto inorganic particles or integrating modified nanoparticles into polymer matrices [1]. These materials have various technical applications, including sensors, solar energy conversion, electrochemical capacitors, information storage, optical signal processing, EMI shielding, battery alternatives, and conducting polymer composites with enhanced characteristics [2]. Numerous studies have focused on harnessing the electrical conductivity of polymers, such as in fuel cells and supercapacitors, for use as electrocatalysts. Electrochemical capacitors, commonly called supercapacitors, have attracted significant attention due to their remarkable power density and substantial capacity. Extensive research has been conducted on several

derivatives of Polythiophene (PTh) and other conducting polymers, such as polyaniline (PANI), polypyrrole (PPy), polyacetylene (PA), and poly (p-phenylenevinylene) (PPV). These materials have exhibited process benefits and favorable mechanical properties, rendering them appropriate for energy storage applications. Polythiophene is a widely sought-after substance for optoelectronic and integrated sensor applications because of its excellent electrical conductivity, impressive optical properties, and extraordinary environmental resilience compared to other conducting polymers [3].

Metal oxide semiconductors such as ZnO, TiO_2, SnO_2, WO_3, Fe_2O_3, etc., are favored as electrode materials for pseudo-capacitors due to their rapid redox kinetics and high capacitance. However, using gas-sensing applications also provides significant advantages[4]. In semiconductor materials composed of metal oxides, pure and doped SnO_2 exhibit numerous applications in gas sensors [5]. The research on nanocomposites of organic and inorganic metal oxides has focused on studying their electrochemical performance, stability, and conductivity. Exceptional materials with more applications [6]. Empirical data has demonstrated that sensors constructed from conductive polymers display a short period for their response when functioning at typical ambient temperature. Using organic fuels and other chemicals has become essential for societal and industrial survival. They produce many harmful, toxic, flammable exhaust fumes, such as nitrogen oxides (NOx). H_2S, NH_3, Cl_2, etc. in the atmosphere[7]. These noxious gases, Nitrogen oxides (NOx, x=1, 2), are a major class of pollutants that are emitted into the environment by automobiles, residences, and companies. Direct inhalation of nitrogen dioxide gas can result in lung inflammation and a weakened ability to resist respiratory infections. A significant factor contributing to acid rain is the presence of nitrogen oxides in the atmosphere, a form of air pollution. Gas sensors have gained significant attention due to the growing awareness of the importance of cleanliness, healthcare, and pollution control. Specifically, there is a strong interest in detecting hazardous, flammable, and poisonous exhaust gases at the part per million (ppm) level. Scientists have dedicated a significant amount of time over the past thirty years to refine gas sensor systems capable of detecting hazardous substances such as these[8].

The current investigation is facilitated through the chemical polymerization of organic-inorganic composite materials, consisting of PTh as the organic constituent, SnO_2 as the inorganic constituent, and multi-walled carbon nanotubes (MWCNT) as the inorganic component. Nanocomposite-based gas sensors have been created and extensively tested for gas-sensing applications. The results indicated that the hybrid materials exhibited superior sensor response, quicker response time, and shorter recovery time in detecting NO_2 at parts per million (ppm) level.

2. EXPERIMENTAL

Polythiophene prepared from thiophene monomer at room temperature is prepared using a chemical method. Firstly, thiophene of 1 ml monomer mixed with 35 ml chloroform CHCl3 is used secondly 3.7 g of iron chloride $FeCl_3$ dissolved in 90 ml of chloroform $CHCl_3$. The results have been mixed with different concentrations of MWCNT and SnO_2. The plumper is placed on top of the magnetic stirrer at a rotational speed of 500 to 1000 RPM for homogeneity. Finally, the results are filtered and dried to make powder. To make a composite, 0.9 g of Polythiophene is reinforced by the chemical method by MWCNTs: SnO_2 with various concentrations of MWCNTs (0.5,0.7and 0.9) g: SnO_2 (0.1).

Aluminum masks with a thickness of 105 nm are deposited in sensor films by thermal evaporation films, which appeared uniform and strongly adherent. The operating temperature of the thin film nanocomposite is determined by subjecting it to a temperature range of 25 to 200 degrees Celsius while simultaneously exposing it to 129 parts per million of nitrogen oxide. The sensitivity of the nanocomposite is subsequently estimated. The identification of phases and determination of crystallite size are conducted by collecting XRD data on the samples, including pure and composite materials. This is done using a Philips X-ray diffractometer, Model PW 1710, with Cu Kα radiation. The powder-

XRD data is collected in the 2θ range of 10-80◦ using step scan mode. The step width is set to 0.02, and the step time is 2.40 S. The emission of electromagnetic waves from the area Utilized a field-emission scanning electron microscope (FE-SEM) to analyze the specimen's morphology. The nanostructure film is analyzed using the Hitachi FE-SEM model S-4160, while FTIR analysis is conducted using solid KBr.

3. RESULTS AND DISCUSSION

The results of nanocomposites with various MWCNTs content and structure have been studied by testing. Figure 1 shows the XRD pattern of nanocomposite that exhibits peak exhibited with the reported value of SnO_2 (JCPDS 41-1445) and graphite (002) reflections (Joint Committee for Powder Diffraction Studies (JCPDS) No. 01-0646) at 2θ= 26.5, 33.8, 37.8, 51.7, 54.6,61.8 and 78.7, by the (110), (101), (111), , (211), (220),(310) and (321) plans respectively, which return to SnO_2. We notice the disappearance of some SnO_2 peaks with an increased ratio of MWCNTs, while the peak of MWCNTs overlaps with a peak of (110) SnO_2. The presence of MWCNTs makes the peaks of SnO_2 expand and weaken, indicating the presence of MWCNTs.The average crystallite size of SnO_2 is about 26 nm [9].

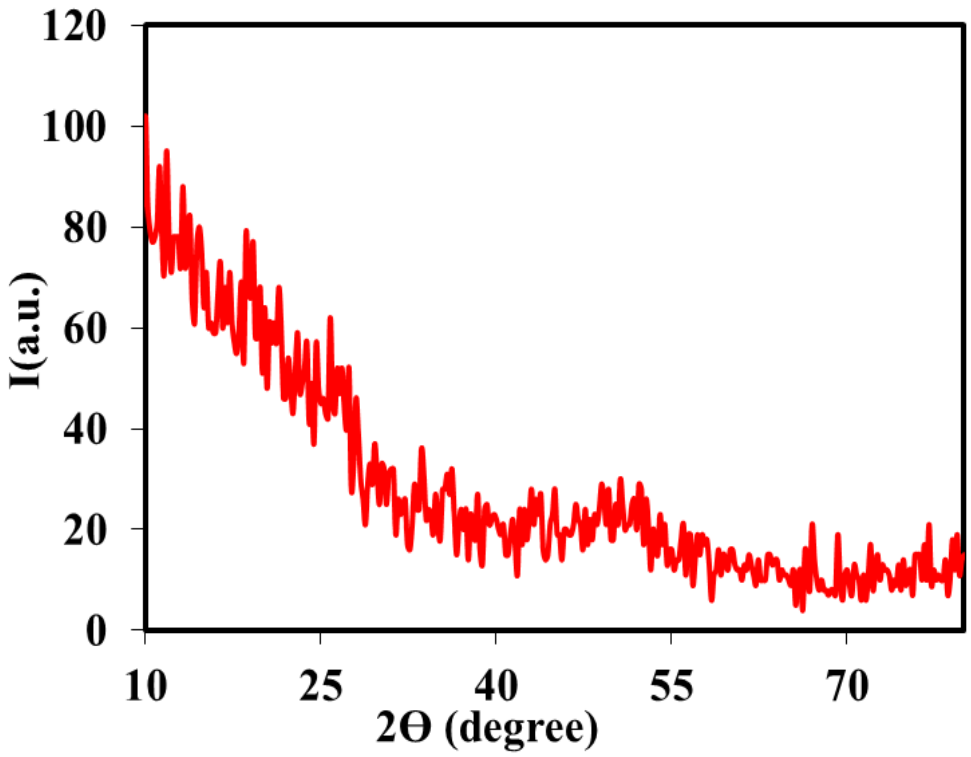

Figure 1 XRD Pattern of PTh.

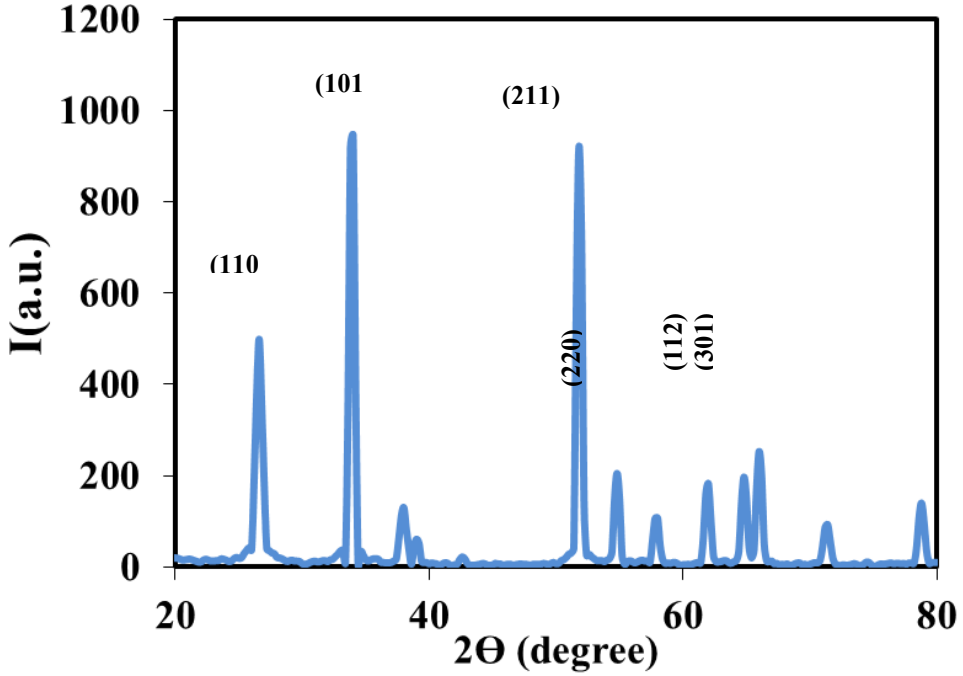

Figure 2 XRD Pattern of SnO_2.

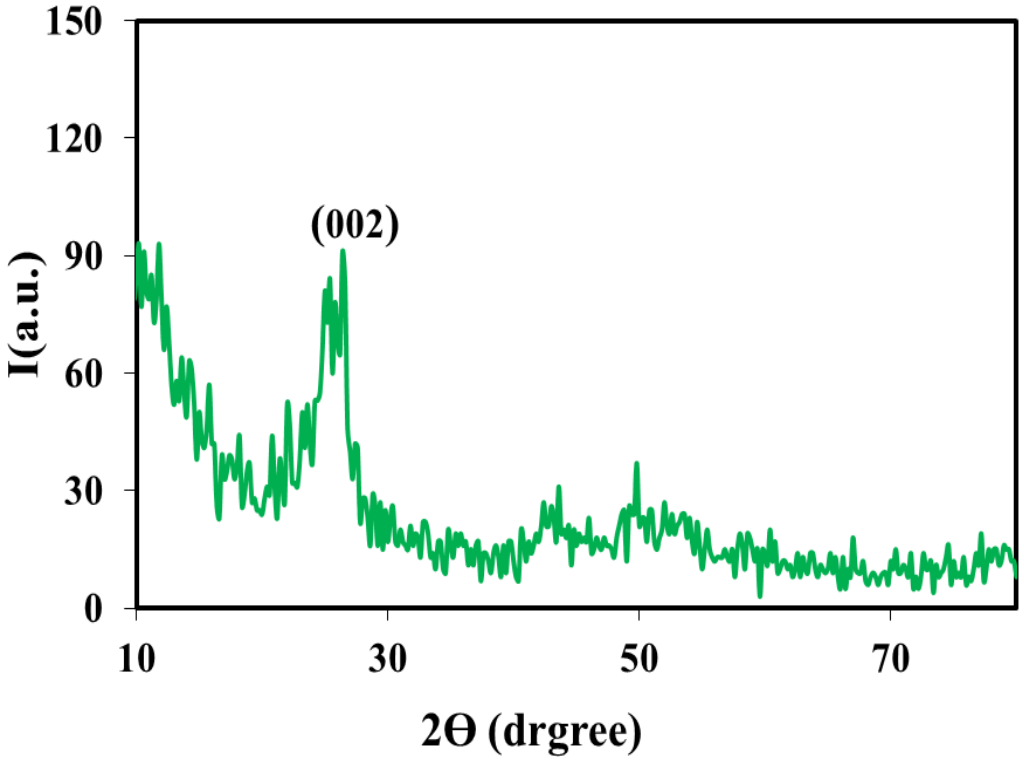

Figure 3 XRD pattern of MWCNTs.

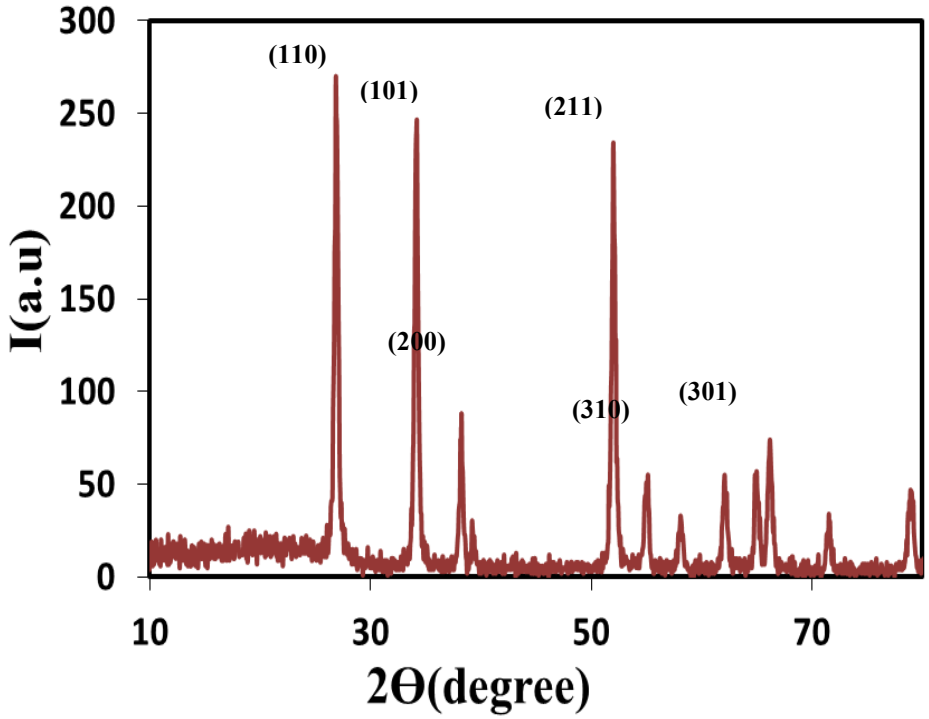

Figure 4 XRD pattern of nanocomposites.

FE- SEM image of nanocomposite It can be seen from Figure 2 that the Shape of the particles exhibits comparatively independent nanofibrous structure with an average diameter of around 37-84 nm and slightly rough surface and a little aggregate adhere into an agglomeration of 500 nm in size, may be due to the interaction [10].

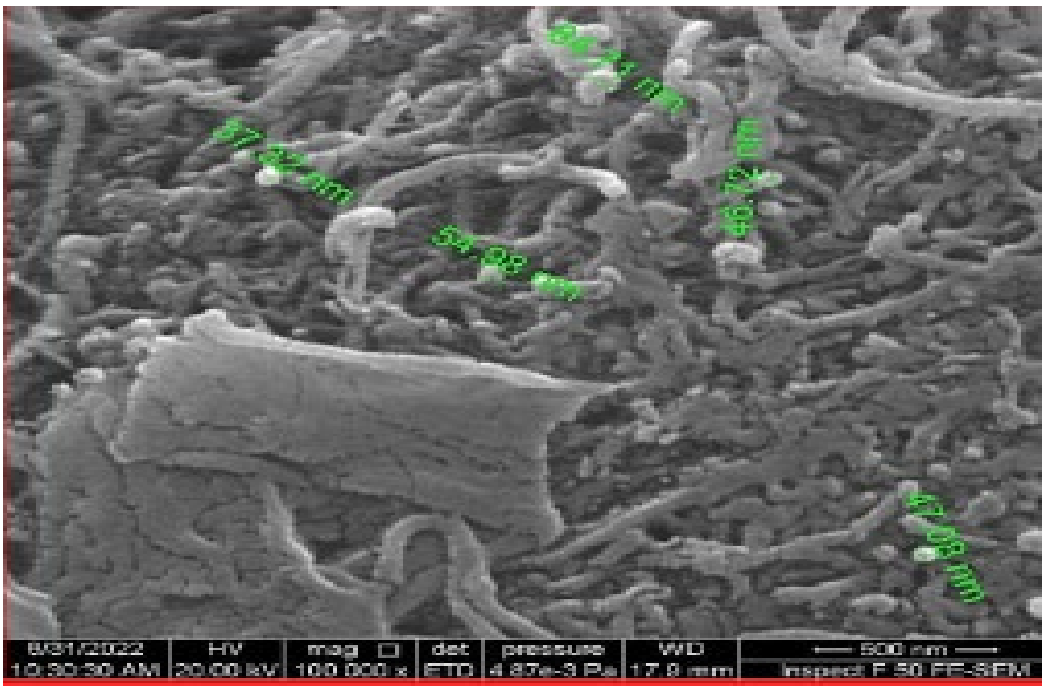

Figure 5 FE-SEM of PTh: 0.1g MWCNTs.

In Figure 3, the particles had irregular Shapes; the average particle size of polythiophene particles is approximately 70.24 nm, with some particles agglomerated [11].

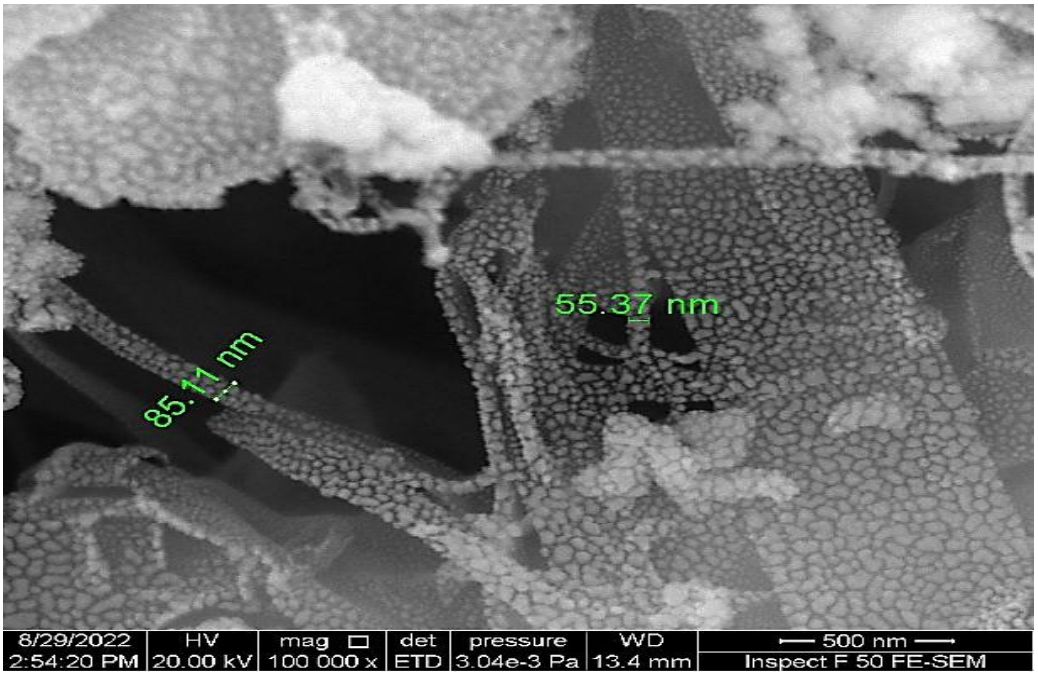

Figure 6 SEM images of PTh: 0.7 g SnO_2

Figures 4, 5, and 6 depict pictures of the PTh: MWCNT: SnO_2 nanocomposite obtained using FE-SEM. The morphology of the samples depicted in Figures 4 to 6 exhibited a disordered arrangement of nanotubes with a lack of alignment. The nanotubes exhibited visible agglomeration, with many regions showing a high degree of tight adhesion. The performance is elucidated by examining both spherical and semi-spherical geometries and the understanding that carbon nanotubes (CNTs) aggregate due to strong intrinsic van der Waals forces. Where the average diameter is about 54.48 nm and 38.33 nm, respectively. Figure 6 shows FE-SEM images of samples PTh: MWCNT: SnO_2(Additive ratios 0.9g:0.1g). it observed that the small nanoparticles are arranged like random chains with average size (31.84 and 34.07) nm, respectively [12].

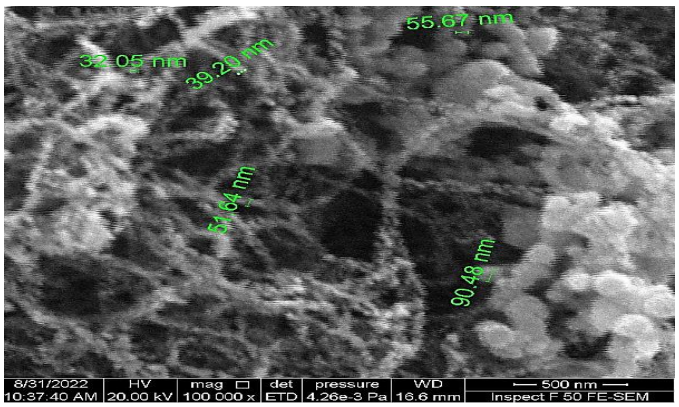

Figure 7 SEM images of images of PTh: MWCNT: SnO_2 (Additive ratios 0.5g: 0.1g).

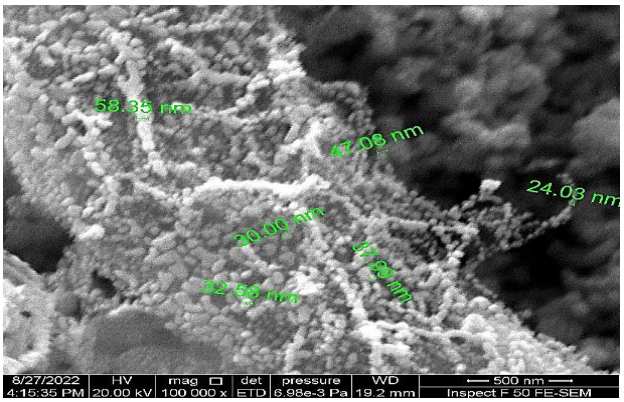

Figure 8 SEM PTh: MWCNT: SnO_2 (Additive ratios 0.7g: 0.1g).

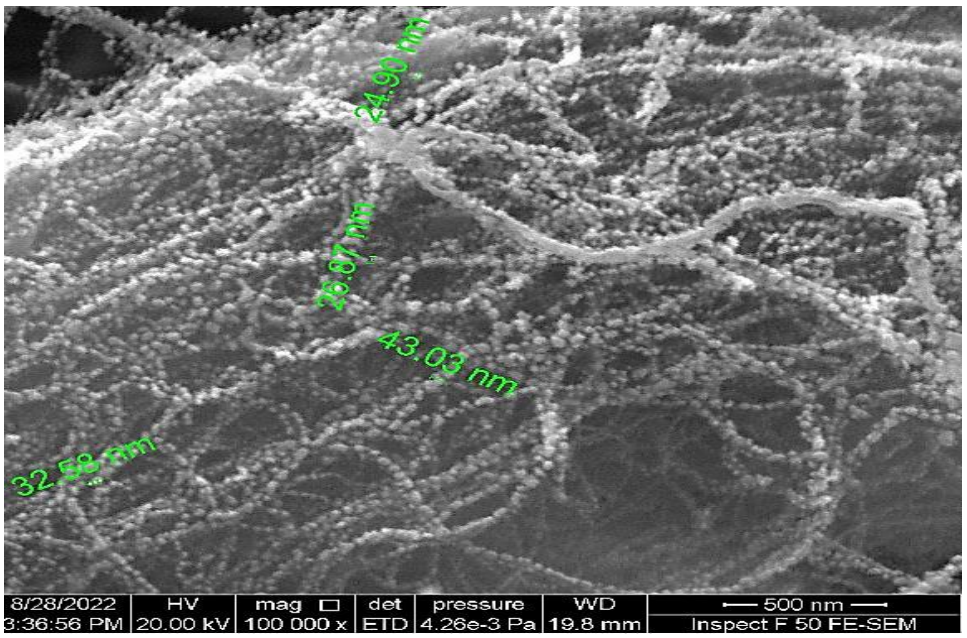

Figure 9 SEM images of PTh: MWCNT: SnO_2 (Additive ratios 0.9g: 0.1g).

Figure 7 shows the FTIR spectra of the nanocomposite with an additive ratio of 0.7g:0.1g. The overall intensity of the O-H band (3423 and 3429 cm^{-1}) is reduced. The band at 709 cm^{-1} is created by the out-of-plane bending of C-H bonds in 2, 5-substituted thiophene rings. The reduced intensity of the peaks at 709 and 696 cm^{-1} might be attributed to the bending mode of the C-S bond. However, this phenomenon is mainly caused by the interfacial trapping between the surfaces of PTh and MWCNTs. The presence of the O-Sn-O bond and the ring deformation mechanism of C-S-C bonds are the probable causes for the bands observed at around 514, 511, and 468 cm^{-1}, respectively. The band at 1419 and 1427 cm^{-1} is attributed to the C-H group. Vibrational modes associated with MWCNTs are identified at a wavenumber of 1575 cm^{-1} [13,14].

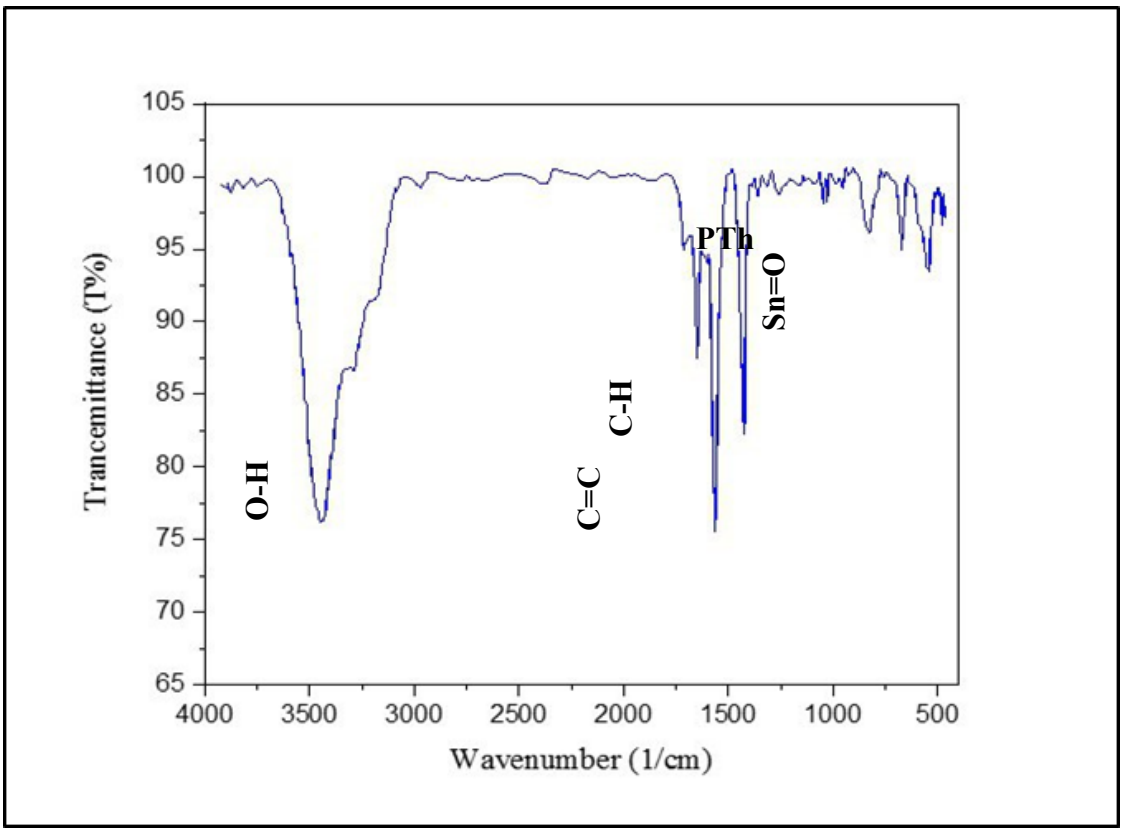

Figure 10 FTIR of nanocomposite.

Figures 8 and 9 demonstrate the variation in sensitivity of the PTH+MWCNT and PTH+SnO_2 films on the glass base as the temperature ranges from 25 to 200 degrees Celsius. Figure 9 displays the PTH/MWCNT and SnO_2 films in various combinations deposited on a glass substrate. A ratio of NO_2 to air is employed for the sensing test, and a bias voltage of 3V is applied to the sensors of all the samples. The equation below calculates the sensitivity factor (S%) when you modify the temperatures [11]. The higher sensitivity may be attributed to the optimum surface roughness, porosity, large surface area, and significant oxidation rate.

Figure (8) shows the sensitivity variation as a temperature function for PTH+MWCNT and PTH+SnO_2 fabricated sensors. The PTH+MWCNT sample sensed NO_2 gas from room temperature up to 200C, with low sensitivity, where the maximum sensitivity equals 3.33% at room temperature[15,16]. The PTH+SnO_2 sample sensed NO_2 gas above 150C to 200C, with Appropriate sensitivity, where the maximum sensitivity equals 10.8% at 150 C [17,18].

Figure (9) shows the variation of the sensitivity as a function of temperature for mixture PTH+MWCNT (0.5-0.7-0.9): PTH+SnO_2 (0.1) fabricated sensors, respectively. The mixture PTH+MWCNT: PTH+SnO_2 samples show higher sensitivity to NO_2 gas from room temperature up to 200C, where the sensitivity increased with increasing operation temperature[19]. The maximum sensitivity equals 62% at 150C for PTH+MWCNT (0.7): PTH+SnO_2 (0.1).

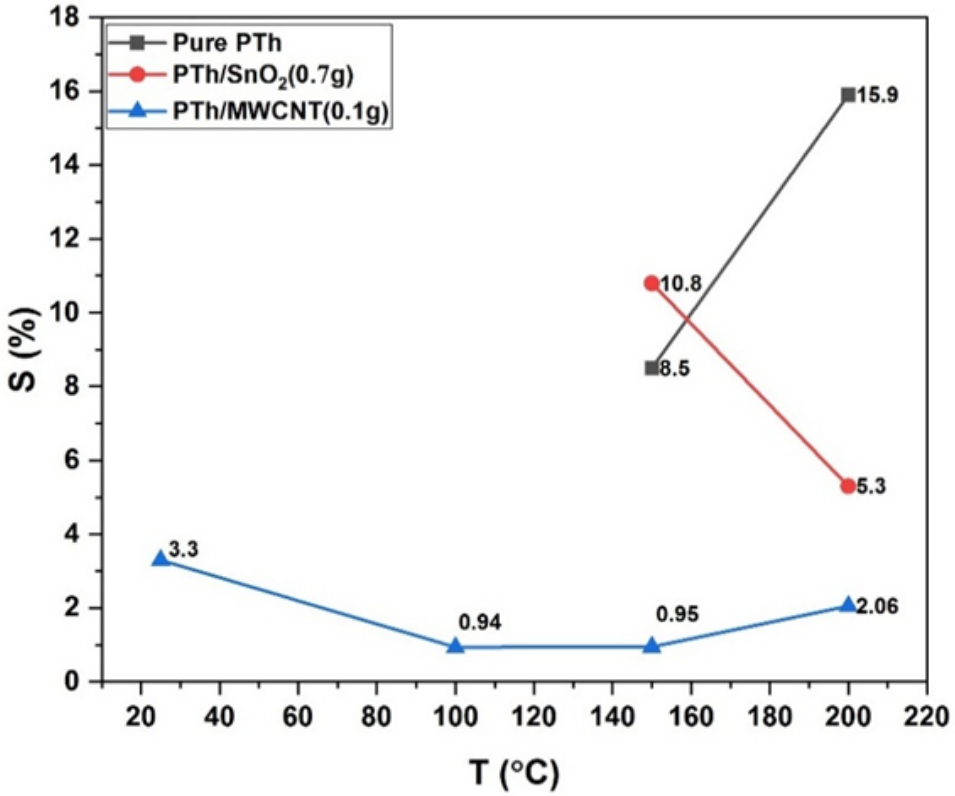

Figure 11 The sensitivity as a function of the operating temperature for PTH+MECNT (0.1) and PTH+SnO_2 (0.7) fabricated sensors.

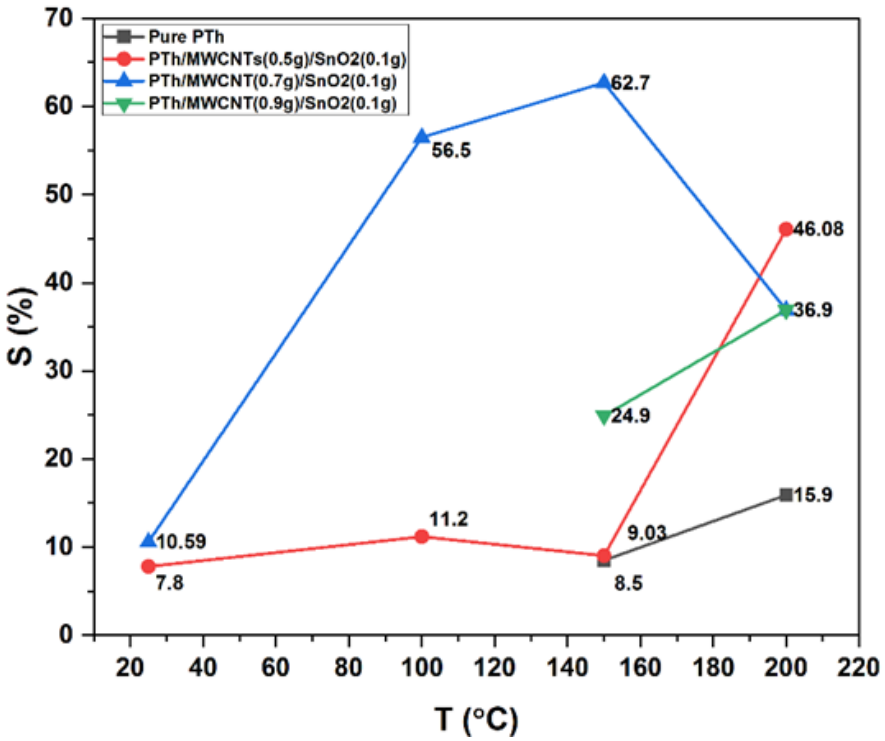

Figure 12 The sensitivity as a function of the operating temperature for different mixtures of PTH+MECNT and PTH+SnO_2 fabricated sensors.

Various combinations of PTH+MWCNT: PTH+SnO_2 samples have been examined, along with the response and recovery timeframes of PTH+SnO_2 and PTH+MWCNT fabricated samples in connection to NO_2 gas. Every test is conducted at a distinct working temperature of 25 to 200 degrees Celsius, with a bias voltage of 3 volts. Figures (10, 11) depict the results. The data illustrates the durations for the artificially created sensor to respond and recover at different operating temperatures. The response and recovery time diminish as the operation temperature increases. The sample with the lowest grain size had the shortest response and recovery time among all the other samples. The response and recovery time are reduced when the amount of oxygen concerning argon is raised. Raising the oxygen flow while preparing sensor samples reduced the amount of oxygen sticking to the surface and removed conduction electrons from the region near the surface. This created a surface layer with fewer electrons, which increased the number of sites available for adsorption and resulted in a quicker reaction time. This agreement pertains to [18].

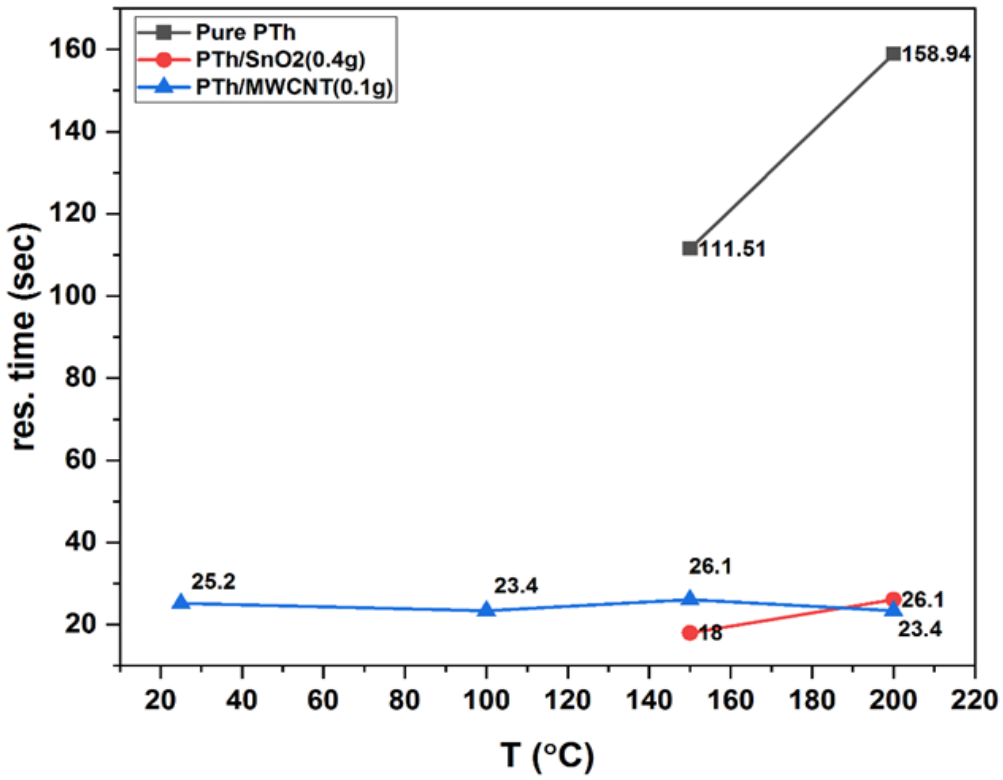

Figure 13 The variation of response time time for PTH+MECNT (0.1) and PTH+SnO_2 (0.7) fabricated sensors.

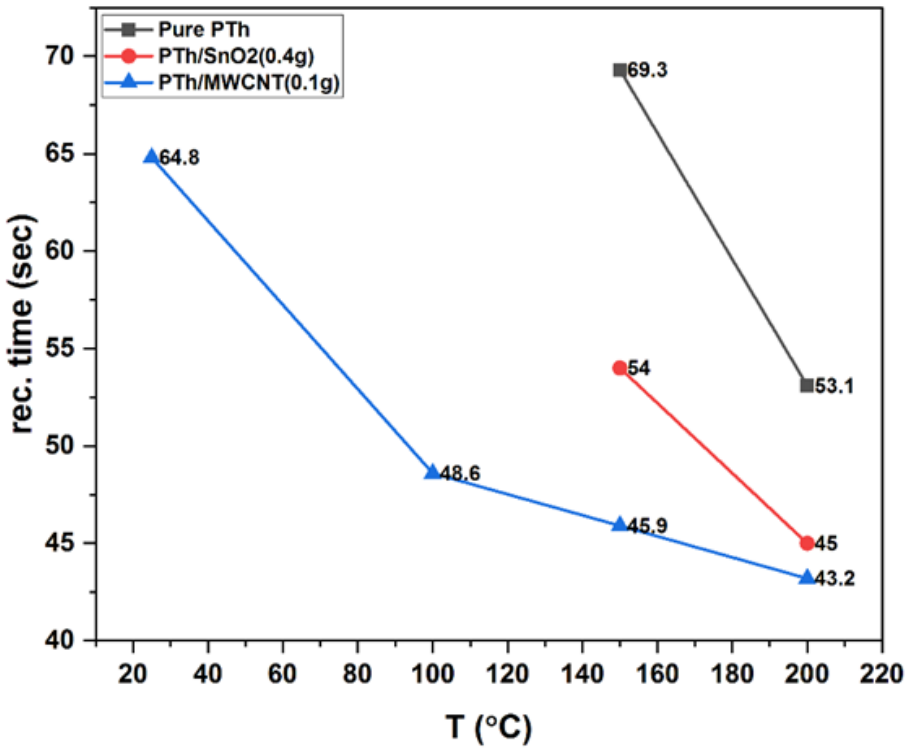

Figure 14 The variation of recovery time for PTH+MECNT (0.1) and PTH+SnO_2 (0.7) fabricated sensors.

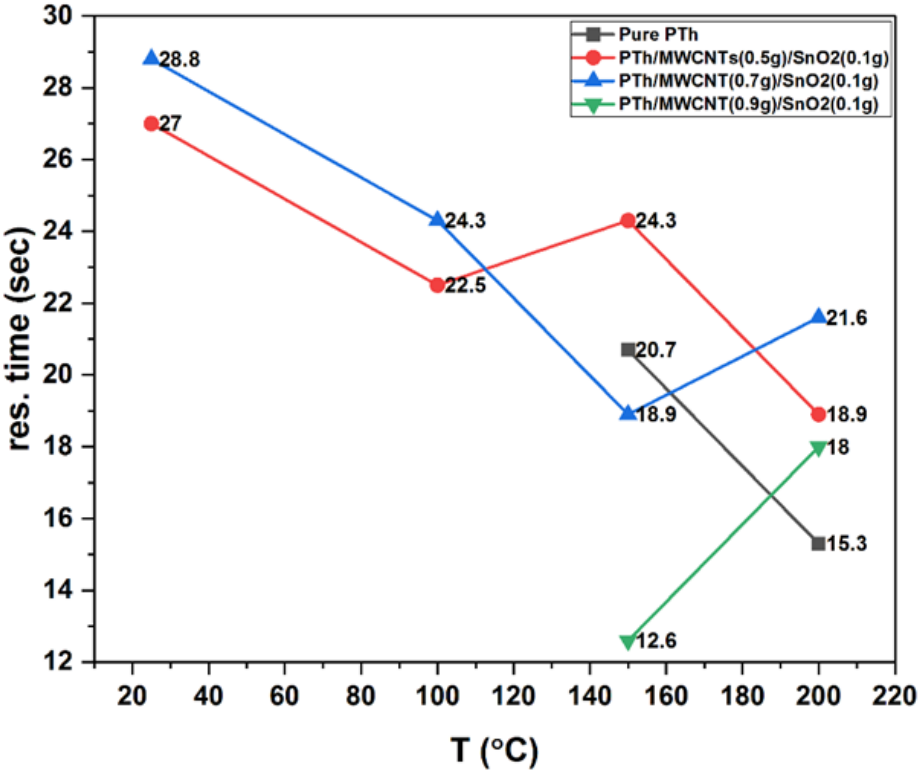

Figure 15 The variation of response time for different mixtures of PTH+MECNT and PTH+SnO_2 fabricated sensors.

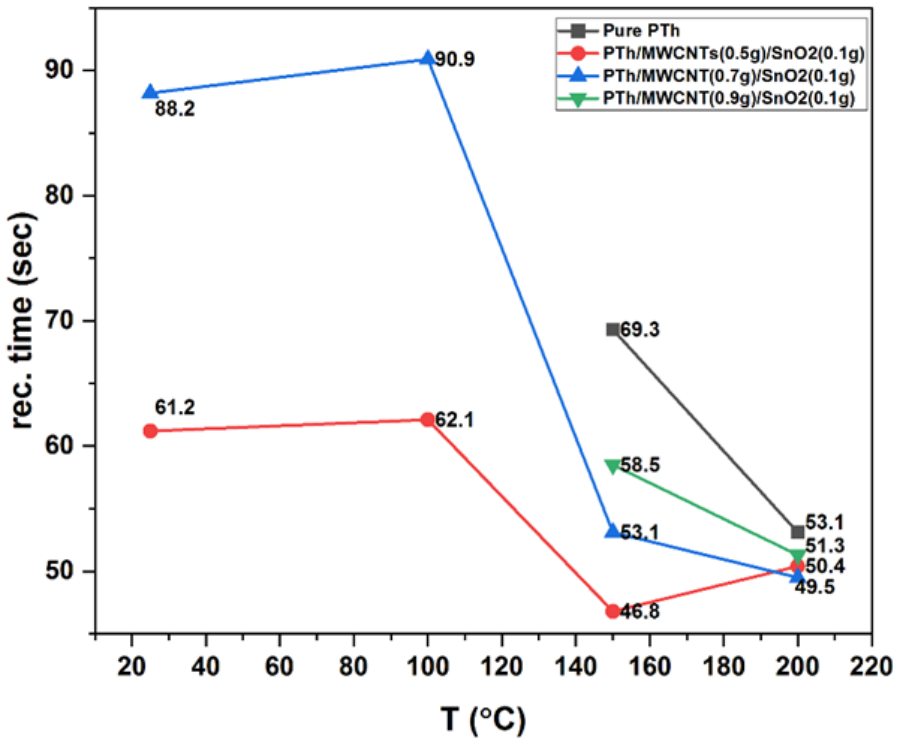

Figure 16 The variation of recovery time for different mixtures of PTH+MECNT and PTH+SnO_2 fabricated sensors.

The gas sensing technique relies on the surface reaction between oxidizing gases and chemisorbed oxygen. Physisorption and chemisorption are the primary mechanisms by which oxygen can be adsorbed onto a film surface. Chemisorption is the dominant process at high temperatures. Increasing the operating temperature facilitates the acquisition of the activation energy required for the transition from physisorption to chemisorption. It has been shown that there is a positive correlation between temperature and the amount of oxygen adsorbed on the sensor's surface [20, 21]. Within the temperature range of 25 to 200 ºC, the gas-sensing and electrophysical properties of the samples are influenced mainly by molecular and atomic oxygen. The process of adsorbing oxygen onto the metal oxide surface enables the capture of electrons. Consequently, the pure and mixed samples display increased resistance because of the reduced density of charge carriers. The oxygen species that have been preabsorbed ($O^{-}surf$) are subjected to NO_2 gas at an elevated temperature. As the oxygen saturation level increases, the number of electrons bound to the conduction band of the sample also increases, resulting in an elevation of the barrier. This phenomenon reduces the ability of a material to conduct electricity and increases its resistance by enlarging the zone where there is a lack of charge carriers [22]. Figure (12) depicts the time-dependent resistance fluctuation of manufacturing samples exposed to NO_2 in ambient air while the bias voltage remains constant at 3V. The testing chamber is used to introduce the NO_2 into the samples. Before the gas opening, a state of stability is reached in the sensor resistance. This state is attained by directly measuring the resistance over time. The gas is currently being released to facilitate its combination with the air present in the chamber. We activated the gas once the resistance had abruptly reached a stable state. The original instance of resistance is later rekindled. The nature of the interaction between the gas molecules and the surface atoms of the sensing film determines the sensor's gas-sensing capability. The structural fault critically determines the surface's reactivity [24].

This phenomenon may occur due to the surface becoming saturated with NO_2 gas, resulting in a quick decrease in resistance until it reaches a saturation point when the gas is introduced. When the gas supply is terminated, the resistance reverts to its initial state. This could be because the sample structure has a higher proportion of p-type multi-walled carbon nanotubes (MWCNT) compared to n-type tin dioxide (SnO_2) [23-25]. The nature of the interaction between the gas molecules and the surface atoms of the sensing film determines the sensor's gas-sensing capability. For the surface to exhibit reactivity, a structural defect must exist [26-31].

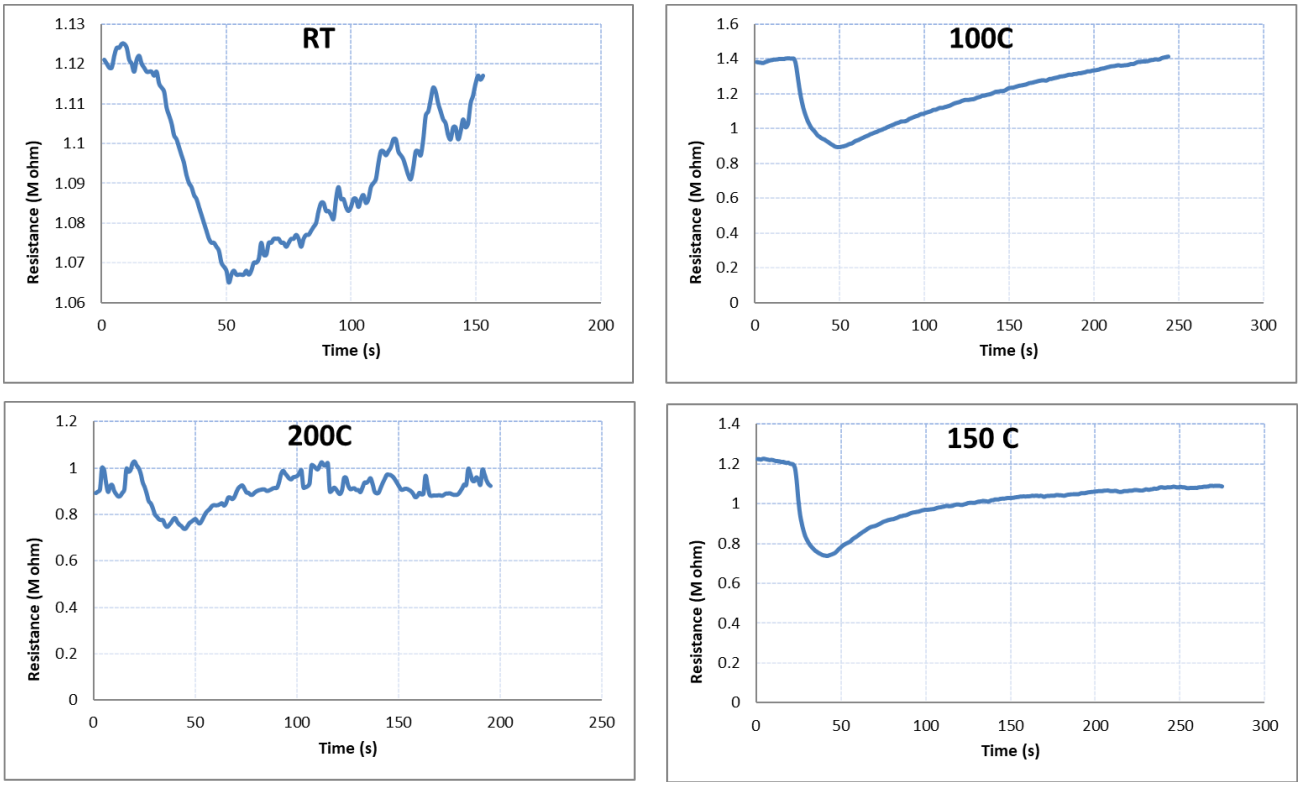

Figure 17 The variation resistance with time for different operation temperatures of NO_2 gas for MS (0.7-0.1).

4. CONCLUSIONS

From the results achieved, the following can be concluded: The chemical oxidation method is effective in preparing the PTh polymer. At the same time, it is successful in preparing nanocomposites. The results of the structural properties (XRD) confirmed the presence of sharp diffraction peaks belonging to SnO_2 and MWCNTs with varying crystalline sizes. Fourier Transform Infrared (FTIR) spectroscopy was employed to study the chemical structure of the bonds, ultraviolet-visible spectroscopy to study the optical properties, field emission scanning electron microscopy (FE-SEM) to study the surface properties, and testing of the nanocomposite as NO_2 gas sensors with different temperatures.

References

[1] J.M. Hatamzadeh, Y. Omidi, Prog. Polym. Sci. 47 (2015) 26 https://doi.org/10.1016/j.progpolymsci.2015.02.004
[2] H.Z.A., Y.L. Xie, Y.X. Wang, L.P. Mo, Y.Y. Yang, Z.Y. Zhang, Mater. Chem. Phys. 114 (2009) 990 https://doi.org/10.1016/j.matchemphys.2008.10.060

[3] K.G. Adhikari, P. Cass, M. Bown, P. Gunatillake, RSC Adv. 5 (2015) 37553 https://doi.org/10.1039/C5RA03037E
[4] Hussian Fakhry, Mohammed RASHEED, Odai N. Salman, Raid A. Ismail, Experimental and Theoretical NANOTECHNOLOGY 10 (2026) 81 https://doi.org/10.56053/10.1.81
[5] Z.J. Guo, H. Xu, B. Cao, ACS Appl. Mater. Interfaces 5 (2013) 7893 https://doi.org/10.1021/am401234k
[6] B.C. Pegu, B.J. Saikia, S.K. Dolui, Polym. Int. 63 (2014) 2061 https://doi.org/10.1002/pi.4747
[7] F.G.F. Cavanagh, L.M. Cavanagh, A. Afonja, R. Binions, Sensors 10 (2010) 5469 https://doi.org/10.3390/s100605469
[8] K.F. Wang, J. Zhang, H. Xia, B. Zhu, Y. Wang, S. Wu, Mater. Sci. Eng. B 150 (2008) 6 https://doi.org/10.1016/j.mseb.2008.03.006
[9] D.A. Manurung, R.V. Asri, L.A. Yuliarto, B. Nugraha, B. Sunendar, Indones. J. Chem. 18 (2018) 344. https://doi.org/10.22146/ijc.26612
[10] N.M. Abdullah, N. Demon, S.Z.N. Halim, I.S. Mohamad, Polymers 13 (2021) 1916 https://doi.org/10.3390/polym13121916
[11] W.F. Gu, T.M. Swager, J. Am. Chem. Soc. 130 (2008) 5392 https://doi.org/10.1021/ja710100m
[12] M.A. Salam, M.S. Makki, M.Y. Abdelaal, J. Alloys Compd. 509 (2011) 2582 https://doi.org/10.1016/j.jallcom.2010.11.037
[13] H.A. Ahmad, F. Mohammad, Materialia 14 (2020) 100868 https://doi.org/10.1016/j.mtla.2020.100868
[14] J.G.V. Rajendran, Mater. Lett. 139 (2015) 116 https://doi.org/10.1016/j.matlet.2014.10.112
[15] R.A.A. Ibrahim, F.T. Ibrahim, E.M. Nasir, J. Phys.: Conf. Ser. 1660 (2020) 012093. https://doi.org/10.1088/1742-6596/1660/1/012093
[16] B.S.S. Bhajantri, R.F. Chavan, C. Sakthipandi, J. Polym. Res. 28 (2021) 251 https://doi.org/10.1007/s10965-021-02563-4
[17] B.S.S. Pinjari, D.V. Nakate, U.T. Singh, P.R. Gogate, J.B. Naik, A.B. Pandit, Chem. Eng. Process. 74 (2013) 115 https://doi.org/10.1016/j.cep.2013.09.003
[18] A.N. Naje, R.R. Ibraheem, F.T. Ibrahim, Photonic Sensors 6 (2016) 153 https://doi.org/10.1007/s13320-016-0287-8
[19] Raghdi, M. Heraiz, M. Rasheed, A. Keziz, Journal of the Indian Chemical Society, 101 (2024) 101413. https://doi.org/10.1016/j.jics.2024.101413
[20] S.R.R. Shinde, V.R. Shinde, C.D. Lokhande, Sens. Actuators B 133 (2008) 296 https://doi.org/10.1016/j.snb.2008.02.016
[21] A.Z.A. Ko, T.G. Ko, J.H. Oh, IEEE Sens. J. 5 (2005) 817 https://doi.org/10.1109/JSEN.2005.848153
[22] K.D.B. Sharma, A.K. Yadav, J.B. Yadav, V.B. Patil, R.S. Devan, A.A. Jatratkar, S.D. Pawar, Sens. Actuators B 244 (2017) 522 https://doi.org/10.1016/j.snb.2016.12.066
[23] H. K. Aity, M. Rasheed, E. Dhahri, A. A. Hateef, T. Saidani, Journal of Materials Science, 61 (2026) 6226. https://doi.org/10.1007/s10853-026-12241-w
[24] T. Saidani, S. Mokhtari, M. Rasheed, H. Lahmar, M. Trari, Journal of the Indian Chemical Society, 103 (2026) 102499. https://doi.org/10.1016/j.jics.2026.102499
[25] M. RASHEED, A. Khaleefah, Materials Chemistry and Physics, 353 (2026) 132112. https://doi.org/10.1016/j.matchemphys.2026.132112
[26] S. S. Batros, M. Rasheed, H. K. Aity, A. A. Hatef, T. Saidani, Materials Chemistry and Physics, 355 (2026) 132243. https://doi.org/10.1016/j.matchemphys.2026.132243
[27] A. I. A. Ali, M. RASHEED, Experimental and Theoretical NANOTECHNOLOGY 10 (2026) 277. https://doi.org/10.56053/10.s.277
[28] A. Khaleefah, M. RASHEED, Experimental and Theoretical NANOTECHNOLOGY 10 (2026)

Exp. Theo. NANOTECHNOLOGY 10 (2026) 693-707
289. https://doi.org/10.56053/10.s.289
[29] Z. S. Ahmed, M. RASHEED, H. S. Ahmed, Experimental and Theoretical NANOTECHNOLOGY 10 (2026) 329 https://doi.org/10.56053/10.s.329
[30] Z. S. Ahmed, M. RASHEED, H. S. Ahmed, Experimental and Theoretical NANOTECHNOLOGY, 10 (2026) 343 https://doi.org/10.56053/10.s.343
[31] A. I. A. Ali, M. RASHEED, Experimental and Theoretical NANOTECHNOLOGY 10 (2026) 239 https://doi.org/10.56053/10.s.239